



OPEN

## Distinct proteomic profiles of plasma-derived extracellular vesicles in healthy, benign, and triple-negative breast cancer: candidate biomarkers for liquid biopsy

G. H. Tamarindo<sup>1,2</sup>, A. A. Novais<sup>3</sup>, B. M. Frigieri<sup>1,4</sup>, D. L. Alves<sup>1,4</sup>, C. A. de Souza<sup>5</sup>, A. Amadeu<sup>1</sup>, J. C. da Silveira<sup>5</sup>, F. F. Souza<sup>6</sup>, N. A. Bordin Jr<sup>7</sup>, L. G. A. Chuffa<sup>8</sup> & D. A. P. C. Zuccari<sup>1</sup>✉

Extracellular vesicles (EVs) derived from plasma, measuring up to 150 nm, act as molecular messengers transmitting critical information to recipient cells, making them valuable candidates for liquid biopsy applications in cancer diagnostics. Triple-negative breast cancer (TNBC) is particularly challenging due to its aggressive nature, metastasis potential, and limited treatment options. This study aimed to identify EV-associated proteins in blood samples that could serve as potential TNBC biomarkers. Using mass spectrometry-based proteomic analysis, we detected unique and differentially expressed proteins across healthy individuals, patients with benign breast conditions, and those with TNBC. While EVs size and concentration showed no differences, the proteomic profile varied significantly among these groups. Several immune-related proteins were found exclusively in healthy individuals but were diminished in both benign and malignant cases. We also assessed the impact of surgery on EVs protein content and identified Histone H2A as a TNBC-specific marker present before surgery. Its expression was further validated through immunohistochemistry and Western blotting in TNBC biopsies and cell lines. Notably, surgical intervention enhanced immune response pathways in TNBC patients. In conclusion, liquid biopsy has the potential to serve as a non-invasive tool for TNBC diagnosis and monitoring, revealing a post-surgery molecular landscape that supports combining immunotherapy with mastectomy.

**Keywords** Liquid biopsy, Breast cancer, Immunotherapy, Extracellular vesicles, TNBC, Proteomics, Surgical intervention, Histone H2A

Breast cancer remains one of the five leading causes of cancer-related mortality among women worldwide<sup>1</sup>. The majority of cases are positive for estrogen and progesterone receptor (ER+ and PR+, respectively). However, patients with human epidermal growth factor receptor 2 (HER2+) overexpression or triple-negative breast cancer (TNBC; ER-, PR- and HER2-) face significantly poorer prognoses<sup>2</sup>. TNBC accounts for approximately

<sup>1</sup>Molecular Investigation of Cancer Laboratory (MICL), Department of Molecular Biology, Faculdade de Medicina de São José do Rio Preto/(FAMERP), São José do Rio Preto, SP 15090-000, Brazil. <sup>2</sup>Brazilian Biosciences National Laboratory, Brazilian Center for Research in Energy and Materials (CNPEM), Campinas, SP 13083-100, Brazil.

<sup>3</sup>Institute of Health Science (ICS), Universidade Federal de Mato Grosso (UFMT), Sinop, MT 78550-728, Brazil.

<sup>4</sup>Institute of Biosciences, Letters and Exact Sciences (IBILCE), UNESP, São José do Rio Preto, SP, Brazil. <sup>5</sup>Laboratory of Molecular Morphophysiology and Development (LMMD/ZMV), University of São Paulo, Pirassununga, SP, Brazil.

<sup>6</sup>Department of Veterinary Surgery and Animal Reproduction, School of Veterinary Medicine and Animal Science, FMVZ, São Paulo State University (UNESP), Botucatu, SP 18618-681, Brazil. <sup>7</sup>Hospital de Base, FAMERP, Faculdade de Medicina de São José do Rio Preto/(FAMERP), São José do Rio Preto, SP 15090-000, Brazil. <sup>8</sup>Department of Structural and Functional Biology, Institute of Biosciences, UNESP - São Paulo State University, Botucatu, São Paulo 18618-689, Brazil. ✉email: debora.zuccari@famerp.br

15 to 20% of all breast cancer cases, and its limited therapeutic options are often ineffective<sup>3</sup>. This challenge has driven extensive research over the past decade, including efforts by our group, to explore novel alternatives for treatment and prevention<sup>4–8</sup>. However, TNBC's molecular complexity<sup>9</sup> contributes to its resistance to multiple therapies, reinforcing its aggressiveness and poor prognosis. Indeed, the molecular landscape of different breast cancer subtypes is increasingly being used to refine diagnostic accuracy and optimize treatment selection<sup>10</sup>. In this context, exploring the distinct molecular milieu of TNBC may enable earlier detection and facilitate the development of more effective therapeutic strategies.

In recent years, liquid biopsy has gained significant attention due to its non-invasive and painless nature<sup>11</sup>, emerging as a promising tool for cancer detection and staging, including in breast cancer<sup>10,12</sup>. Among the key components of blood are plasma-derived extracellular vesicles (EVs), structures enclosed by a lipid bilayer, ranging from 40 to 1000 nm in size<sup>13</sup>. While EVs naturally occur in physiological processes, their morphology and cargo can be altered in cancer, as tumor cells actively release them to mediate long-distance communication. These vesicles have been shown to transport proteins, lipids, RNA, miRNA, and even organelles, which can be internalized by recipient cells, triggering downstream signaling events that contribute to metastasis niche formation<sup>14</sup>, immune evasion<sup>15</sup> and enhanced chemoresistance<sup>16</sup>. Given their role in tumor progression, EVs represent a promising avenue for cancer surveillance and staging, even though further studies are needed to translate these findings into clinical practice.

In breast cancer, plasma-derived EVs, mainly exosomes (30–150 nm), have been documented to promote immunosuppression by inducing CD8+ lymphocyte exhaustion<sup>15,17</sup> and macrophage type 2 polarization, as well as contributing to metastasis, drug resistance<sup>18</sup>, tumor microenvironment remodeling<sup>19</sup>, angiogenesis<sup>20</sup> and metabolic reprogramming<sup>21</sup>, including through the transfer of breast cancer-derived EVs to neutrophils<sup>22</sup>. The functional significance of EVs in breast cancer has also been leveraged to distinguish different breast cancer subtypes and tumor stages based on their cargo and composition<sup>23</sup>. While lipids<sup>24</sup>, miRNAs, and circular RNAs<sup>25</sup> have been proposed as potential biomarkers, proteins have been extensively explored in the context of liquid biopsy<sup>26</sup>. Considering this scenario and the potential utilization of EVs, we hypothesized that the protein cargo of plasma-derived EVs differs among healthy individuals, patients with benign tumor, and those with TNBC, as well as before and after surgical intervention. For this purpose, we performed a comprehensive proteomic analysis using mass spectrometry to identify unique and differentially expressed proteins enriched in key molecular pathways associated with tumor progression and metastasis. Additionally, we validated a specific target in TNBC tissue and human breast cancer cell lines by assessing its protein expression levels, evidencing its potential as diagnostic biomarker.

## Materials and methods

### Experimental design

Twenty-nine women consented to participate in this study and were assigned to one of the following groups: Healthy (no breast cancer detected), Benign (diagnosed with a benign breast tumor), and TNBC (diagnosed with triple-negative breast cancer, defined by negative staining for ER, PR, and HER2). Patients in the TNBC group were followed up for 9 to 12 months after tumor excision, allowing for two sample collection time points: one at diagnosis and another after surgery. Inclusion criteria were based on a pathological diagnosis following the classification of breast cancer subtypes as preconized by Goldhirsch and colleagues<sup>2</sup>. TNBC cases were confirmed through immunolabeling of core biopsy sections for ER, PR, and HER2, while benign tumors were identified by the absence of neoplastic cells. Healthy tissue samples exhibited no pathological alterations. These characterizations were performed at the Pathology Division core held at the Hospital de Base in São José do Rio Preto (São Paulo, Brazil). Informed consent was obtained from all participants and/or their legal guardians before sample collection. The study was conducted in accordance with the Declaration of Helsinki and all experiments were performed in compliance to the guidelines and regulations determined by the institutional Human Research Ethics Committee of the Faculdade de Medicina de São José do Rio Preto. The study was registered under Protocol 28462920.8.0000.5415 and approved under number 4.007.723. Biometric information and biopsy immunohistochemistry data were presented in Tables 1 and 2 of the Supplementary Material. A summary of our methodology and experimental design was shown in Fig. 1.

### EVs isolation

A total of 3 to 5 milliliters of blood was collected by the staff of the Ambulatory Care Facility of the Hospital de Base in São José do Rio Preto (São Paulo, Brazil) and immediately processed for sample preparation. EVs isolation was performed as previously described by Novais and colleagues<sup>23</sup> with modifications. Briefly, blood samples were collected in ethylenediaminetetraacetic acid (EDTA)-coated tubes and centrifuged at 2500 g for 15 min at room temperature to separate supernatant containing platelet-poor plasma. Then, plasma was subjected to a three-step sequential centrifugation at 4 °C, being the first at 300 g for 10 min to remove cells, then the supernatant was collected and centrifuged at 2500 g for 10 min to pellet and discard cellular debris, and finally at 16,500 g for 30 min to remove EVs larger than 150 nm. The resulting plasma supernatant was immediately stored at –80 °C to preserve EVs integrity for downstream analyses.

EVs were purified using size exclusion chromatography (SEC) method with qEVoriginal Columns (#ICO-35, IZON), specifically designed to isolate EVs ranging from 35 to 350 nm, optimal for exosome separation. Briefly, the columns were placed in the holder and flushed twice with filtered PBS at room temperature before sample loading. Subsequently, 500 µL of plasma was added to the system for EVs purification. After sample loading, EVs were eluted in 1.2 mL in PBS and stored in a new tube for downstream analyses.

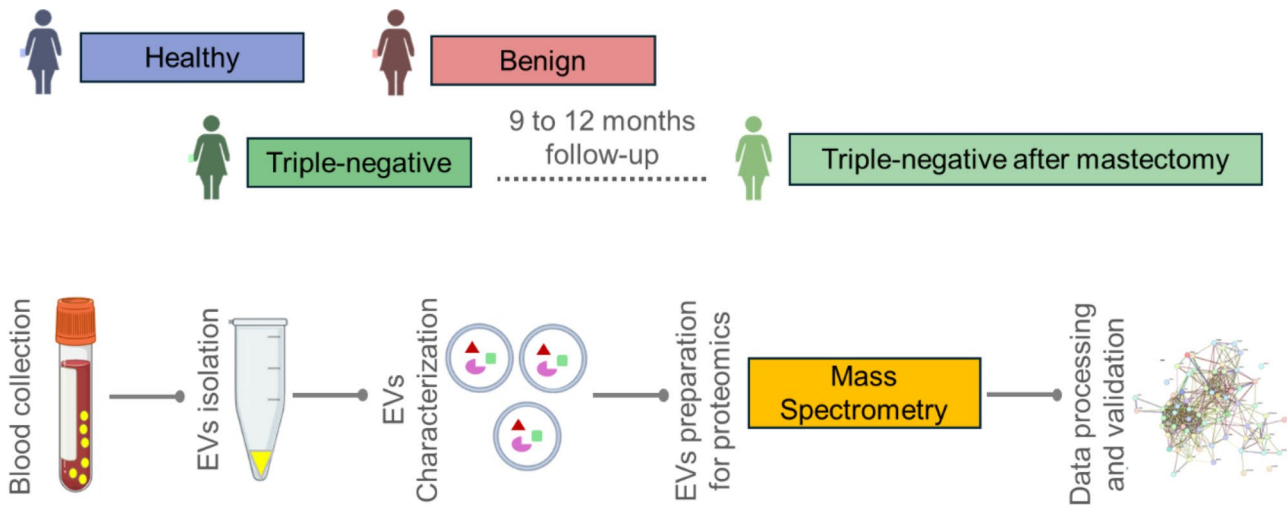


**Fig. 1.** Methodological approach for EVs proteomics analysis. Patients were assigned to Healthy, Benign, and Triple-negative (TNBC), based on the diagnoses issued by the Pathology Core. Blood samples were collected prior to any therapeutic intervention, ensuring that EVs were isolated as the first step after collection. These isolated EVs were then subjected to proteomics analysis using mass spectrometry. The data was processed and analyzed to explore the differential protein profiles across the groups.

### EVs characterization

To determine the size and concentration of EVs, Nanoparticle Tracking Analysis (NTA) was performed. Briefly, exosome-enriched pellets were resuspended and diluted in calcium- and magnesium-free PBS (1:500). The suspended particles were subjected to a laser beam, and five 30-second videos were captured, tracking Brownian motion at 20x magnification (sCMOS in Camera Level 15 at 37 °C). Particles were individually analyzed using Nano-Sight software (NS300; NTA 3.4 Build 3.4.003; Malvern, Worcestershire, UK). The hydrodynamic diameter was calculated using the Stokes-Einstein equation, with size reported as the mean of mode diameter (nm) and concentration expressed as mean of particles per mL plus standard deviation (SD).

To validate EVs isolation, we used flow nano-cytometry in random samples. First, isolated EVs were centrifuged at 20,000 g for 30 min at 4 °C. The samples were then incubated for 2 h at room temperature with shaking using conjugated antibodies against CD81-PE (1:20; ab 81436, Abcam), Syntenin-PE (1:50; sc-515538, Santa Cruz Biotechnology) and ALIX-PE (1:50; sc-53540, Santa Cruz Biotechnology). Following incubation, permeabilization was performed with 0.001% Triton (1:1 v/v) for 15 min at room temperature. PBS with antibody served as a negative control. Flow cytometry was conducted using CytoFLEX (Beckman Coulter, USA) with gain and threshold adjusted to bead size (100–300 nm), following the manufacturer's instructions. The gating strategy was defined based on the negative control, and EVs marker expression was reported as the number of positive events per microliter of sample.

For additional validation, we performed Transmission Electron Microscopy (TEM) on randomly selected EVs samples, as described previously<sup>23,27–30</sup>. Briefly, the exosome-enriched pellets were resuspended in a fixative solution containing 0.1 M sodium cacodylate, 2.5% glutaraldehyde, 4% paraformaldehyde (pH 7.2–7.4) for 2 h at room temperature. Next, the fixed samples were diluted in 2 mL of ultrapure water, followed by centrifugation at 119,700 g for 70 min at 4 °C. The resulting EVs pellet was resuspended in ultrapure water and placed onto a pioloform-coated copper grid for 5 min. The grid was then stained with 2% aqueous uranyl acetate. Images were acquired at 140,000 X magnification using a FEI 200 kV (Tecna 20, emitter LAB6) at the Multiuser Electron Microscopy Laboratory, University of São Paulo (Ribeirão Preto, Brazil).

### Proteomic analysis

EVs-containing pellets isolated from plasma samples were processed for protein extraction at the Animal Reproduction Laboratory, UNESP (Botucatu, São Paulo, Brazil). Briefly,  $10^7$  EVs were lysed with RIPA buffer containing protease inhibitor cocktail (Aprotinin 1 µg/mL, Leupeptin-1 µg/mL, PMSF 35 µg/mL, and EDTA 0.8 mM), followed by sonication and centrifugation at 10,000 g for 30 min at 4 °C. The supernatant was desalting using 3 kDa Amicon® ultrafilters (#UFC5003, Millipore Corporation) with 50 mM ammonium bicarbonate buffer. Total protein concentration was quantified using the Pierce™ 660 nm Protein Assay (#22660, ThermoFisher Scientific) at 545 nm. For tryptic digestion, 4 µg of protein was loaded onto an SDS-PAGE gel and run until the sample entered the separation gel (30–40 min). A single protein band was excised from the gel and subjected to dehydration with 100% acetonitrile for 10 min, rehydrated in a reductive solution (20 mM dithiothreitol, #161–0611, BioRad) at 56°C for 40 min, and then alkylated (55 mM iodoacetamide, #RPN-6302 V, GE) at room temperature for 30 min. Proteins were digested in-gel using trypsin at 20 ng/µL, 1:50 trypsin/substrate ratio (#V511, Promega), overnight. We chose to perform protein digestion for proteomics in gel to prevent the detergents contained in the RIPA buffer used for EVs lysis from interfering with mass spectrometry. Peptides

were concentrated and resuspended in 0.1% trifluoroacetic acid (TFA, #299537, Sigma-Aldrich), followed by desalting with Zip Tip (#ZTC18M, Millipore Corporation). The final elution was performed in 50% acetonitrile.

Proteomic analysis was carried out entirely by the facility core at the Max Feffer Genetics of Plants Laboratory (Escola Superior de Agricultura Luiz de Queiroz, University of São Paulo, Piracicaba, São Paulo, Brazil). Proteomic analysis was conducted using a nanoElute nanoflow coupled to a hybrid trapped ion mobility spectrometry-quadrupole time-of-flight mass spectrometer (timsTOF Pro). For analysis, 1 µL of sample (200ng of digested peptides) was injected into a Bruker FIFTEEN C18 column (1.9 µm, 150 mm x 75 µm). Reverse-phase gradient (Solvent A: 0.1% AF, 99.9% H<sub>2</sub>O; Solvent B: 0.1% AF, 99.9% CH<sub>3</sub>CN) was established in a nanoflow liquid chromatography system and separated under a flux of 250 nL·min<sup>-1</sup>. Column temperature was kept at 50 °C. Chromatographic run was 60 min (2–30% of Solvent B for 55 min, raised to 95% at 56 min and kept for 4 min). The column was coupled online to timsTOF-Pro with ions source CaptiveSpray. The temperature of capillary ion transfer was adjusted to 180 °C. Ion accumulation was allowed for 123ms and the separation performed by mobility were obtained with a ramp of input potential from – 160 to – 20 V within 123ms. During acquisition, to enable the PASEF method, a full scan Tims-MS experiment was performed (m/z 100–1700) to determine the ion fragmentation, m/z precursor information and motility. Mono-loaded precursors were excluded from their position in m/z-ion motility plan and those that reached 20,000 a.u. were dynamically excluded for 0.4 min. Operational mode of TIMS-ToF, MS and PASEF were controlled and synchronized with OtofControl 5.1. Unless otherwise stated, all instruments and consumables were purchased from Bruker Daltonik, Germany. The raw data files (.d) were processed in MaxQuant software version 2.4.0.0, integrated with the Andromeda search engine<sup>31,32</sup>. Default settings were applied for data from the TIMS-TOF Pro mass spectrometer. The fragment ion mass tolerance was set to 0.5 Da, with a minimum peptide length of seven amino acids. The false discovery rates (FDRs) for peptides and proteins were set to 1%, and a criterion of at least one unique peptide was required for protein identification. After data processing, relative abundance values for all identified proteins were obtained. The database used was UP000005640, available at <https://www.uniprot.org/proteomes/UP000005640> (taxonomy *Homo sapiens*), downloaded on March 9, 2023, and containing 82,861 proteins. Proteomic results were filtered using Perseus analysis software (version 2.0.9.0)<sup>33</sup>. Proteins were retained in the abundance matrix only if they had nonzero values in at least 90% of samples from at least one experimental group. Subsequently, a script in R programming language (<https://www.R-project.org/>) was employed to refine the filter based on protein presence in the groups and to normalize the data by total ion count (TIC).

To identify key proteins, processed peak intensities were submitted to Metaboanalyst 5.0<sup>34</sup> to generate heatmaps after Pareto scaling, highlighting the most significant altered proteins. Identified proteins retrieved from the Uniprot database for *Homo sapiens* were displayed using their gene names, while predicted, inferred, or uncertain proteins were indicated by their primary accession numbers. Exclusive and shared proteins were visualized using Venn diagrams (<https://bioinformatics.psb.ugent.be/webtools/Venn/>, accessed on July 30, 2024). For the shared proteins, values were shown as mean of fold-change of TIC intensity and SD. The PANTHER Overrepresentation Test (Released 20240226) was performed using the Reactome database (version 85 Released 2023-05-25, version 86 Released 2023-09-07) with the *Homo sapiens* gene set as a reference<sup>35–37</sup>. Features were analyzed using Fisher's exact test, with a false discovery rate (FDR)<0.05 considered significant. Enrichment scores were reported as – log (p value). To assess protein interaction networks, the protein list was submitted to the STRING database<sup>38</sup>. Finally, exclusive proteins were double-checked in the Uniprot database, and those categorized as having experimental evidence at the protein level, experimental evidence at the transcript level, inferred from homology, or protein predicted were inserted in the color squares. Proteins categorized as uncertain were excluded from further analysis.

### Immunohistochemistry

Paraffin-embedded breast biopsy samples were sectioned into 3–4 µm slices using a microtome. Following histological processing, sections underwent antigen retrieval by incubation in preheated citrate buffer (pH 6.0) at 95°C in a steam pot for 30 minutes. Endogenous peroxidase activity was inhibited by incubating the slides with hydrogen peroxide solution for 15 minutes, followed by two 5-minute PBS washes. Non-specific protein binding was blocked with 3% bovine serum albumin (BSA) for 15 minutes. The sections were then incubated overnight at 4°C in a humid chamber with the primary antibodies anti-Histone H2A (1:600; A3692, ABclonal) and anti-CSTA (1:300; ab166805, Abcam). HRP enzyme marker (Dako Agilent Technologies, Inc.) was added for 15 minutes in the slides, and the reaction was developed using 3,3'-diaminobenzidine tetrahydrochloride (DAB) for 2 min. The slides were counterstained with filtered Harris' Hematoxylin. Negative controls for both proteins were obtained by omitting the antibodies while appendix tissue was used as positive control for Histone-H2A and liver for CSTA. For quantification, at least three images from distinct biopsy slices from different patients were captured using NIKON E200 ECLIPSE LEICA EC3 microscope at 40X magnification ( $n=8$ , TNBC;  $n=1$ , HER2-amplified;  $n=2$ , Luminal). Immunolabeling intensity was quantified using NIH Image J with IHC Profiler plugin, which automatically classified labeled pixels into low positive, positive, and high positive categories. The final IHC score was calculated as: (1 x % low positive) + (2 x % positive) + (3 x % high positive)<sup>39,40</sup>. Values were plotted as mean ± SD.

### Cell culture

Human breast cancer cell line MDA-MB-231 (triple-negative; #HTB-26, ATCC), MCF7 (Luminal; #HTB-22, ATCC) and SK-BR-3 (HER2-Amplified; #HTB-30, ATCC) were cultured in DMEM medium (#D2780, VitroCell) containing glucose at 4.5 g/L supplemented with 4 mM of L-glutamine and 10% fetal bovine serum. The medium was changed every 2–3 days, and cells were sub-cultured using 0.025% trypsin-EDTA when they reached 70–80% confluence. For experiments, cells were seeded at the desired density and allowed to attach to the plate for 24 h.

### Western blotting

Cells were seeded at a density of  $10^6$  cells per 60 mm dish and cultured for 48 h. Afterwards, cells were harvested and pelleted by centrifugation at 300 g for 5 min at room temperature, then washed once with PBS. The cell pellets were lysed in RIPA buffer supplemented with protease and phosphatase inhibitor cocktails for 40 min on ice. Cell debris was removed by centrifugation at 14,000 RPM for 20 min at 4°C, and the supernatant was collected. Total protein concentration was determined using the Pierce™ BCA Protein Assay Kit (#23225; ThermoFischer) at 562 nm in a microplate reader. For SDS-PAGE, 20 µg of protein from each cell lysate was loaded onto the gel for electrophoresis. Proteins were then transferred onto a nitrocellulose membrane using a TransBlot system for 7 min. Non-specific binding was blocked with 5% non-fat dry milk in TBST for 1 h at room temperature with shaking. Membranes were then incubated overnight at 4°C with primary antibodies against Histone H2A (1:500; A3692, ABclonal) or Cystatin A (1:500; ab166805, Abcam) in 5% BSA. For loading control, membranes were incubated with β-actin (1:1000; A5441, Sigma-Aldrich). HRP-conjugated secondary antibodies were added at 1:5000 dilution for 1 h at 4°C. Protein bands were visualized using an ECL system with ChemiDoc (BioRad). Histone H2A and Cystatin A were evaluated in the same membrane after stripping. Values were shown as mean of protein levels to β-actin and SD.

### Statistical analysis

All statistical analyses, except for omics data, were performed using GraphPad Prism software (version 10.3.1). Initially, data normality was assessed using the Shapiro-Wilk and Kolmogorov-Smirnov tests. To compare before and after mastectomy values in the TNBC group, a paired t-test was applied for parametric data and a Wilcoxon matched-pairs signed rank test for non-parametric. For comparison between two groups, an unpaired t-test was performed for parametric data while Mann-Whitney was done for the non-parametric. For comparison across three groups, an ordinary one-way ANOVA test was performed for parametric data, followed by Tukey's multiple comparisons test or the Kruskal-Wallis test for non-parametric data. Values were expressed as mean with  $\pm$  SD.

## Results

### EVs concentration and size did not differ between healthy women and patients with benign or triple-negative breast cancer

Given our previous findings that the amount of EVs may vary across breast cancer subtypes<sup>41</sup>, we first evaluated their concentration and size using NTA assay. Our results showed no significant differences between healthy women, benign cases, and TNBC patients. However, as expected, high variability was observed across individuals (Fig. 2A-D). Flow cytometry confirmed the presence of CD81, ALIX, and Syntenin, well-established EVs markers, in both Benign and TNBC (at diagnosis) groups (Fig. 2E). Additionally, TEM further validated the presence of EVs (Fig. 2F). As previously reported<sup>23</sup>, EVs concentration and size alone may not differentiate

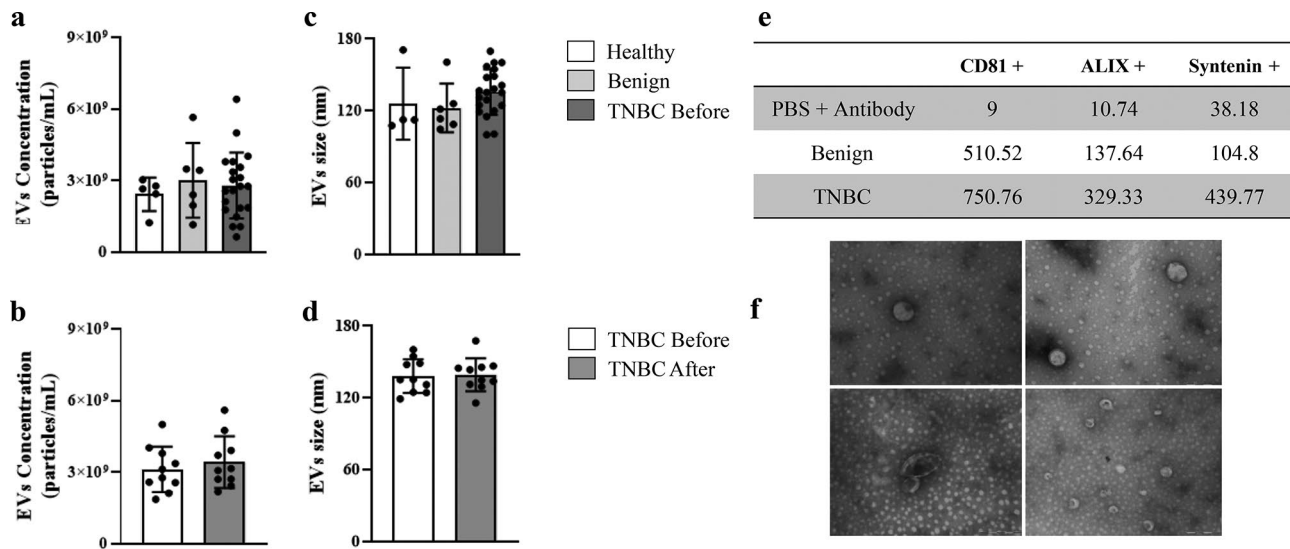


**Fig. 2.** EVs characterization. The concentration of EVs in serum was determined using NTA in the following groups: (a) Healthy, Benign and TNBC (at diagnosis, referred to as TNBC Before) groups, and (b) Levels in TNBC patients Before and After mastectomy. Values were expressed as the mean of particles/mL of blood plus SD. No significant differences in concentration were observed among the groups. EVs size in (c) Healthy, Benign and TNBC (at diagnosis, referred to as TNBC Before) groups, and (d) Levels in TNBC Before and After surgery. Values were determined by NTA assay and shown as the mean of nm plus SD. (e) Flow nanocytometry was used to validate the isolation of EVs by detecting the presence of the markers CD81, ALIX, and Syntenin. Values represent the number of positive events per volume ( $\mu\text{L}$ ) of sample for each marker. (f) Transmission Electron Microscopy (TEM) was performed on random EVs samples, confirming its presence in samples after isolation. Magnification at 140,000X.

between group, but their cargo can be more informative. Therefore, we proceeded with proteomic analysis to characterize EVs protein profile.

### EVs cargo distinguishes healthy, benign, and TNBC patients, revealing potential biomarkers for liquid biopsy

To investigate whether EVs cargo profile differentiate healthy individuals from patients with benign or TNBC tumors, we performed proteomic analysis. The results revealed distinct proteomic profiles among the groups, as illustrated by the heat map of the top 30 ranked proteins (Fig. 3A). A complete heat map displaying all identified proteins was shown in Fig.S1. Next, we identified unique proteins to each group (Fig. 3B). Healthy individuals had the highest number of exclusive proteins in the isolated EVs (75), whereas the Benign group had only two: ZG16B and APOC2. In contrast, the TNBC group had a single exclusive protein, HISTH2B. However, due to methodological limitations, we could not specify which histone variants (HIST1H2BM, HIST1H2BL,



**Fig. 3.** EVs proteomic profile remarkably changes among healthy, benign, and TNBC patients. (A) Heat map displays the top 30 proteins (rows) across samples (columns) from women in the Healthy (purple), Benign (orange), and TNBC (green) groups. (B) Venn diagrams reveal shared and exclusive proteins in each group. Unique proteins in the Healthy group were highlighted in blue, those in the Benign in pink, and in the TNBC in green squares. (C) The top 20 enriched pathways, as identified using the Reactome (version 85 Released 2023-05-25) database, were shown for the Healthy group based on its unique protein set. (D) The network interaction map, retrieved from STRING, illustrates how the proteins within the enriched pathways interact. Values were shown as -log(p-value).

HIST1H2BD, HIST1H2BC, HIST2H2BF, HIST1H2BH, HIST1H2BN, HIST1H2BK, H2BFS, HIST1H2BJ, HIST1H2BO, HIST1H2BB, HIST2H2BE, or HIST3H2BB) was the most abundant in EVs. To determine whether these proteins are involved in specific biological pathways, we conducted enrichment analysis. Significant results were found only for the set of proteins unique to the Healthy group, which were primarily associated with pathways related to immune system regulation and RAF/BRAF signaling, as identified through Reactome enrichment analysis (Fig. 3C). A full list of enriched pathways can be found in Table 3 of Supplementary Material. Figure 3D shows potential network formation and protein interaction among this gene set.

We next examined whether proteins shared between groups exhibited differences in abundance within EVs. A total of 22 proteins were common between the Healthy and Benign groups and those with statistical significance were shown in Fig. 4 while those unchanged in Fig.S2. Ten proteins were significantly overexpressed in the Benign group, with increase of at least 276% in APOC3, IGLC6, FABP5, IGJ, TPII, LCN1, DEFA, LYZ, GGCT, and PIP. In contrast, SERPINB3 and IGHA1 showed an approximately 60% reduction compared to the Healthy patients (Fig. 4A-L). These proteins did not show significant involvement in the enrichment analysis, except for their roles in the Binding and Uptake of Ligands by Scavenger Receptors (R-HSA-2173782.3) and Scavenging of heme from plasma (R-HSA-2168880.3). However, when considering all 22 shared proteins, enrichment analysis highlighted their involvement in pathways associated with immune system regulation and lipoprotein-related metabolism (Fig. 4S). Additionally, these proteins exhibited clustering and potential interaction, as illustrated in Fig. 4T. In contrast, TNBC patients shared only three proteins with the Healthy group, specifically CSTA, HISTH2A, and CASP14, all of which were significantly increased by at least 7.8-fold in the malignant stage (Fig. 4M-O). Importantly, due to methodological limitations, we were unable to determine which specific HISTH2A isoforms were differentially expressed, leaving HIST1H2AJ, HIST1H2AH, H2AFJ, HIST2H2AC, HIST2H2AA3, HIST1H2AD, and HIST1H2AG as potential candidates. These findings suggest that EVs cargo alterations reflect disease progression, with distinct protein expression patterns emerging in the Benign and TNBC stages, underscoring their potential biomarker value in breast cancer detection and classification.

Four EVs proteins were shared among the Healthy, Benign, and TNBC groups. Ubiquitins (Fig. 4P), which could correspond to UBA52, RPS27A, UBB, or UBC (distinction was not possible with our methodological approach), and HBB were significantly increased in the TNBC group (Fig. 4Q). Meanwhile, DCD was elevated in both Benign and TNBC groups (Fig. 4R). In contrast, ACTB remained unchanged across all conditions (Fig.S2).

### Alterations in EVs cargo following tumor excision in TNBC patients

Given the identification of unique proteins in TNBC, we further investigated whether mastectomy would alter the EVs' cargo. Remarkably, hierarchical clustering revealed a distinct post-surgical protein profile, clearly separating each group (Fig. 5A, top 20 proteins; the complete heat map with all proteins was shown in Fig.S3). Tumor excision led to a substantial remodeling of the EVs' cargo, with the emergence of 44 exclusive proteins post-surgery (Fig. 5B). In contrast, only CSTA and HISTH2A were uniquely identified in samples before mastectomy (Fig. 5B). Enrichment analysis linked these post-surgical proteins to pathways involved in lipid metabolism (mainly lipoproteins), immune system regulation, and integrin signaling (Fig. 5C). The complete list of enriched pathways is available in Table 4 of the Supplementary Material. Additionally, these newly identified proteins appeared to interact within a network, as depicted in Fig. 5D.

Next, we interrogated whether the shared proteins were altered by surgical intervention. Despite being detected before and after surgery, the levels of ACTB, HBB, HISTH2B and DCD were significantly reduced, decreasing by at least 80% following mastectomy (Fig. 6A-F).

### HISTH2A and CSTA are elevated in EVs of TNBC patients and expressed in breast cancer cell lines and core biopsies

Considering that CSTA and HISTH2A were either unique or had a sharp reduction in its abundance in our comparisons, we further investigated their expression in triple-negative, HER2-amplified, and Luminal breast cancer tissues using core biopsy samples. Both CSTA and HISTH2A were expressed across all subtypes (Fig. 7A); however, only HISTH2A was significantly elevated in TNBC tissues. To further elucidate this finding, we assessed their protein levels in breast cancer cell lines via western blotting. We analyzed MDA-MB-231 (TNBC), SK-BR-3 (HER2-amplified), and MCF7 (Luminal) cells (Fig. 7B-D). Consistent with our tissue analysis, HISTH2A was highly expressed in MDA-MB-231 cells (Fig. 7B) but was absent in SK-BR-3 and MCF7. Conversely, CSTA was detected in all three cell lines (Fig. 7C), although its expression levels appeared lower in SK-BR-3 and MCF7 cells compared to MDA-MB-231.

### Discussion

EVs serve as molecular conduits for tumor communication, playing a key role in pathways that drive disease progression. In this study, we identified distinct molecular pathways enriched in plasma-derived EVs (exosomes) from healthy individuals, patients with benign tumors, and those with TNBC. These differences underscored important biological processes associated with tumor progression, highlighting potential diagnostic and therapeutic targets for TNBC and benign lesions. By comparing EVs profiles before and after tumor excision in TNBC patients, we observed a shift in their cargo. Notably, unique proteins that were depleted in the presence of the tumor emerged after excision, indicating potential biomarkers for tumor relapse that require further investigation. Lastly, we validated that histone H2A expression is increased in TNBC by analyzing tissue biopsies and established breast cancer cell lines, reinforcing its potential as a TNBC-specific biomarker.

Benign breast tumors, such as fibroadenomas, are characterized by hyperplasia without metastasis and represent the most common type of benign breast lesions<sup>42</sup>. Although fibroadenomas are generally considered non-malignant, an ongoing debate persists regarding their role in breast cancer risk, as they were associated with a 1.77-fold increased likelihood of developing breast cancer compared to healthy women<sup>43</sup>. Herein, we identified

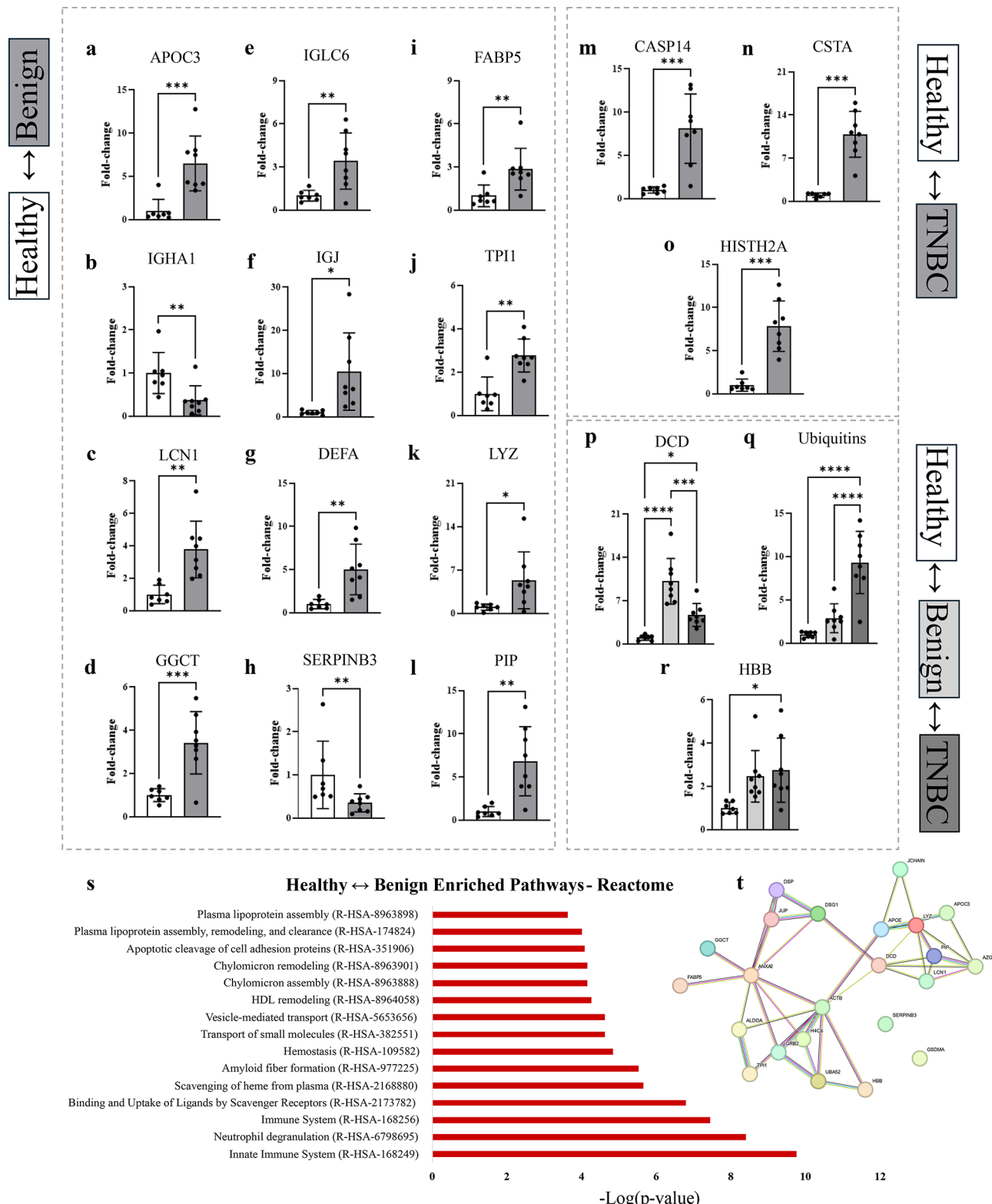


**Fig. 4.** Several shared proteins have distinct abundance and may serve as potential markers for diagnosis. Proteins abundance in EVs are as follows: (A–L) Healthy and Benign; (M–O) Healthy and TNBC; and (P–R) Healthy, Benign, and TNBC. Data shows only the statistically significant proteins. Values show mean of fold-change to Healthy group plus SD. (S) Enriched pathways for all shared proteins among the Healthy and Benign groups (regardless of statistical significance). Enrichment was determined using the Reactome database (version 86 Released 2023-09-07), with values shown as -log(p-value). (T) This panel presents the protein network interaction map for the shared proteins, rendered using the STRING database.

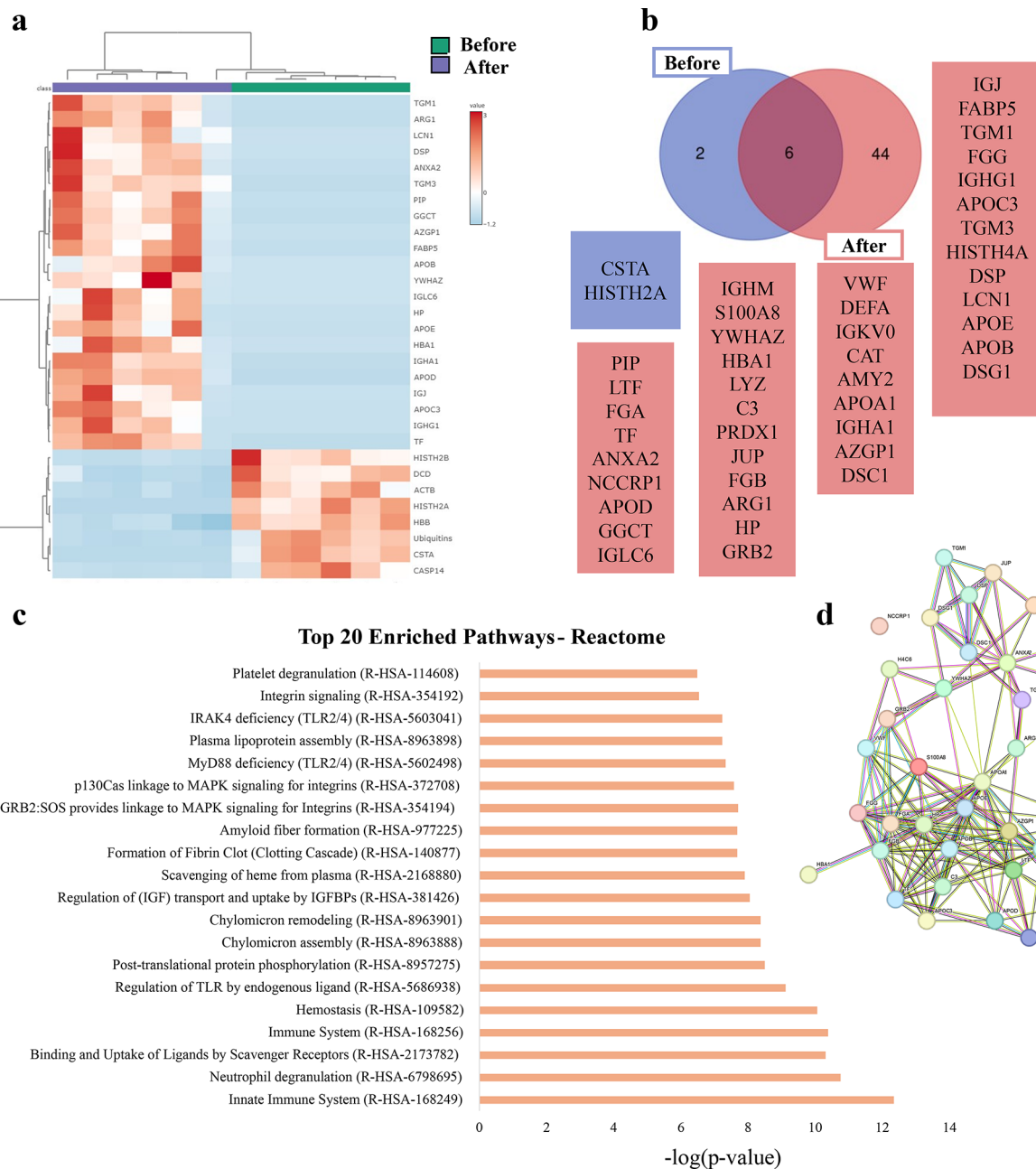


**Fig. 5.** EVs cargo changes in TNBC patients following mastectomy. **(a)** Heat map of proteomic profile of EVs before (green) and after (blue) mastectomy. **(b)** Venn diagram highlighting shared but also unique proteins after tumor excision or not. Blue squares represent proteins exclusive to before surgery EVs, while pink squares indicate proteins unique to EVs after surgery. **(c)** Top 20 enriched pathways associated with the unique proteins observed following mastectomy based on Reactome database (version 85 Released 2023-05-25). Enrichment significance was shown as -log(p-value). **(d)** The protein interaction network, retrieved from STRING database, illustrates the relationship between the unique proteins identified after mastectomy.

exclusive proteins in plasma-derived EVs from healthy women that were absent in patients with benign or malignant tumors. These proteins could serve as potential surveillance markers, offering valuable insights for early detection and risk assessment. Additionally, the enrichment analysis of protein cargo in EVs highlighted predominant pathways in Healthy women that seems suppressed in the other groups. Although proteins directly involved in BRAF and RAF1 signaling were not detected, the signaling due to their fusion was the most enriched pathway. This output may reflect a mechanism in healthy cells to avoid BRAF and RAF1 fusion, a well-known genomic alteration frequently observed in breast cancer. The BRAF V600E mutation, a cancer-promoting factor, promotes cell proliferation and division<sup>44</sup>, and particularly in TNBC, elevated BRAF levels correlate with poor prognosis<sup>45</sup>. This finding is quite relevant when considered alongside with our results showing that proteins in EVs from healthy women are involved in both adaptative or innate immune responses. Notably, TNBC has

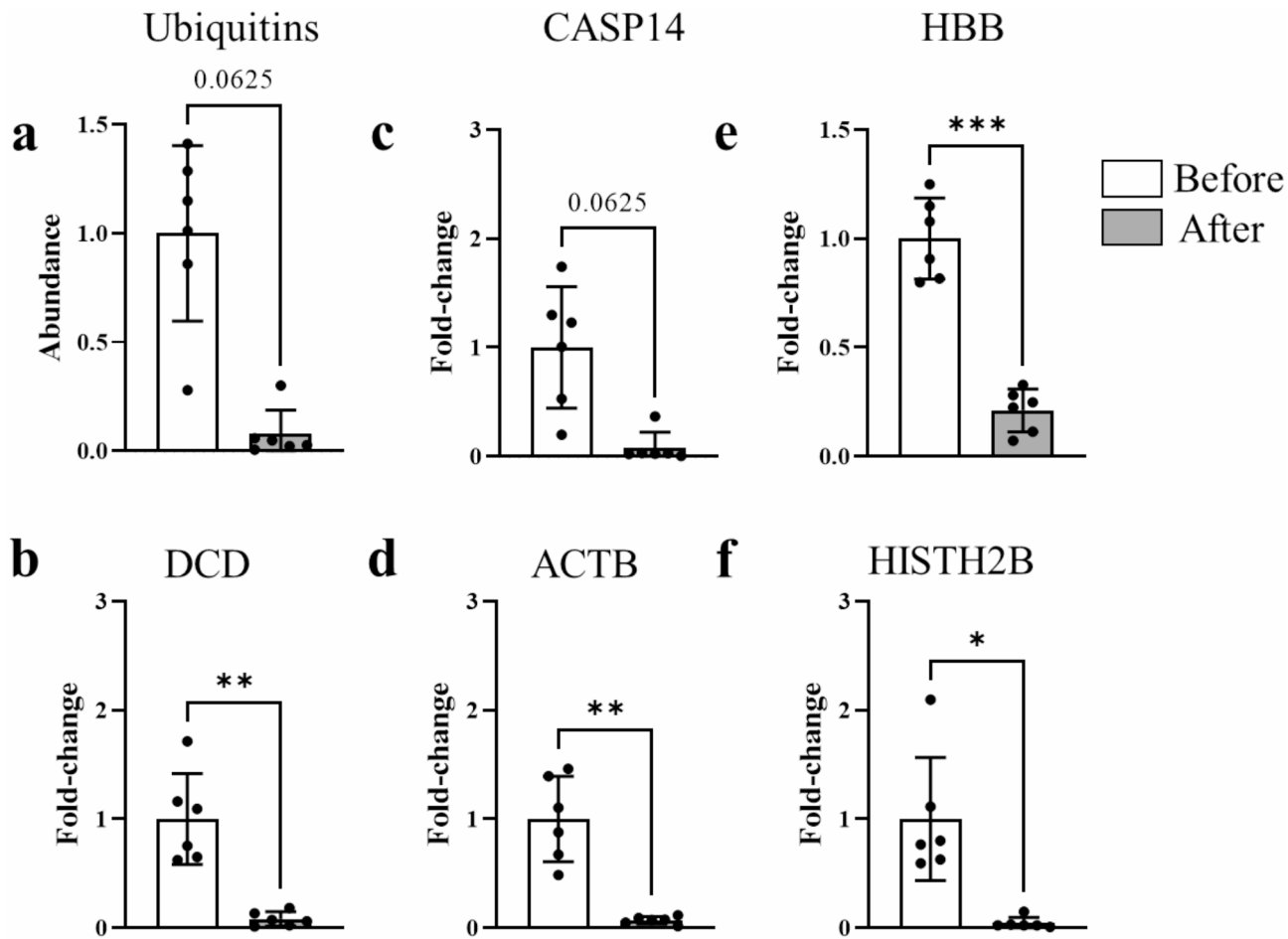


**Fig. 6.** Persistent proteins in EVs cargo of TNBC patients decrease after tumor excision. (a-f) Panels show the decline in persistent proteins detected in EVs from TNBC patients following mastectomy. Protein levels were measured before and after surgery, with values expressed as mean of fold-change relative to pre-surgery levels along with SD.

been reported to modify the immune system<sup>46</sup>, induce CD8 + T cells exclusion via neutrophil extracellular traps (NETs)<sup>47</sup> and to modulate myeloid cell populations, thereby influencing responses to immunotherapy<sup>48</sup>. Taken together, these observations suggest that in healthy individuals, immune surveillance – particularly by innate immune cells - plays a protective role. Moreover, our study supports that TNBC may shift towards immune modulation, facilitating tumor progression and immune evasion.

Despite not being exclusive, most proteins shared between healthy women and those with benign tumors were more abundant in the latter group. Innate and adaptative immune-related pathways remained the most enriched, suggesting active immune surveillance, which may correlate with the lower risk of benign tumors becoming malignant. Among the exclusive proteins found in plasma-derived EVs was zymogen granule protein 16B (ZG16B), a key regulator of T-cell mediated immunity via PD-L1<sup>49,50</sup>, potentially enhancing antitumor response. To our knowledge, this is the first study to propose ZG16B as a liquid biopsy marker for benign breast tumors. Similarly, DCD levels were higher in benign tumors compared to both healthy and malignant plasma-derived EVs. DCD, an antimicrobial peptide usually secreted by eccrine glands, modulates innate immune cells<sup>51</sup>. Brauer and colleagues<sup>52</sup> showed in a mouse model of N-methylnitrosourea-induced breast cancer that DCD levels increased by the fourth week after exposure, coinciding with ductal hyperplasia – a phase that may progress to adenocarcinoma. In this experimental model<sup>52</sup>, DCD levels peaked during the development of palpable mammary carcinomas. In human breast cancer, DCD expression has been correlated with HER2-amplified and Luminal subtypes, with its tumorigenic role linked to HER2 signaling<sup>53</sup>. This may explain why DCD levels were highest in benign tumors, followed by a decrease in TNBC-derived EVs. Taken together, these findings position DCD as a promising biomarker for liquid biopsy, particularly for identifying benign proliferative disorders or the early stages of carcinogenesis. However, this association requires further elucidation.

APOC2, an apolipoprotein, was also found exclusively in benign-derived EVs. Consistently, there was an increase in the abundance of proteins involved in lipoproteins remodeling in benign condition compared to healthy women. Variations in apolipoprotein profiles have been reported across breast fibrotic disease, early-stage cancer, and tumor recurrence<sup>54</sup>. Mosapour and colleagues<sup>55</sup> similarly found that VLDL-C levels were

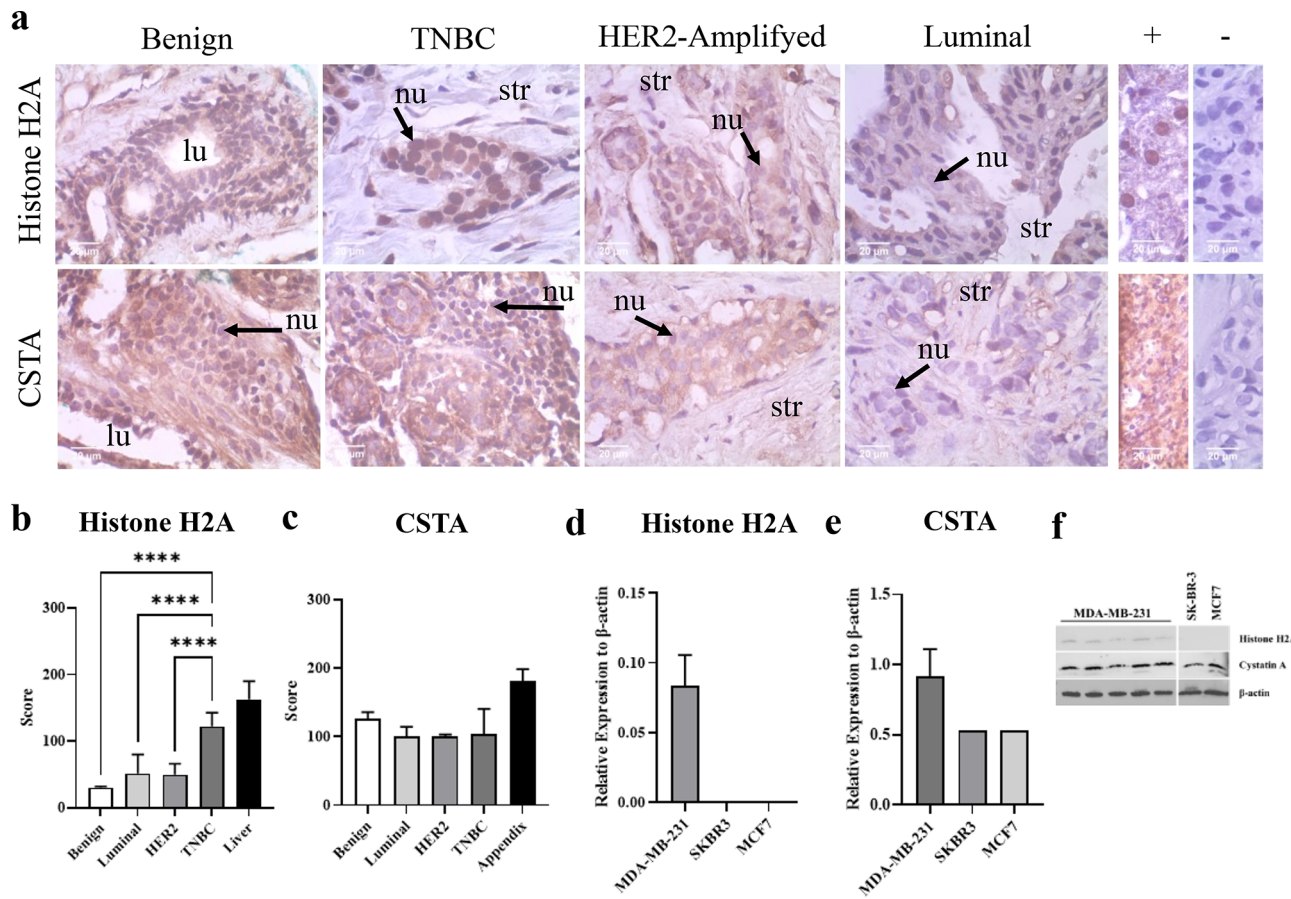


**Fig. 7.** Histone H2A are differentially expressed in TNBC. (a) The left panel displays immunohistochemical staining for Histone H2A (upper row) and Cystatin A (lower row) in core biopsies from TNBC ( $n=8$ ), HER2-amplified ( $n=1$ ), Luminal breast cancer ( $n=2$ ), as well as benign tumors ( $n=1$ ). Positive controls (+): Appendix tissue for CSTA and liver for Histone H2A. Negative controls (-): Samples incubated without the primary antibody were shown in the right panel (last column). Immunolabeling were shown in brown after DAB reaction. Images were captured at 40x magnification, with scale bars representing 20  $\mu$ m. Quantification of Histone H2A (b) and Cystatin A (c) expression across different breast cancer subtypes and benign tissue. Western blot analysis of Histone H2A (d) and Cystatin A (e) in MDA-MB-231 (TNBC), SK-BR-3 (HER2-amplified), and MCF7 (Luminal) breast cancer cell lines. Values were shown as mean of protein levels normalized to  $\beta$ -actin plus SD. (f) Representative Western blot bands, detected using ECL system. Original blots and gels are available in Supplementary Figure S4. Legend: nu – nucleus; str – stroma; lu – lumen; - - negative control; + – positive control; TNBC – triple-negative breast cancer; CSTA – cystatin A; \*\*\*\* –  $p < 0.0001$ .

elevated in both benign and malignant breast tumors compared to healthy women. This increase in triglyceride levels reduce hormone-binding globulin, thereby raising free estradiol levels in the serum<sup>56</sup>. Importantly, the association of lipid metabolism has been as a tumor-promoting alteration in several cancers<sup>57–60</sup> including breast cancer<sup>8,61</sup>. Therefore, lipoproteins modulation may favor benign breast cells proliferation, as these cells are dependent on estrogen through downstream transcription of estrogen response elements (EREs)<sup>62</sup>.

Surgical intervention is among the front-line approaches for TNBC, given the lack of effective targeted therapies, but it can directly impact women's quality of life. Consequently, new diagnostic tools and therapeutic strategies are being actively explored to improve patient outcomes. In our study, we reported HISTH2B as an exclusive protein in TNBC-plasma derived EVs, while Ubiquitins were more abundant in TNBC compared to benign and healthy conditions. This suggests that ubiquitination could be one of the molecular pathways activated in recipient cells. This hypothesis is partially based on evidence that UBA52 depletion, a ubiquitin-ribosomal fusion protein found in our dataset, decreases cell proliferation, and interacts with histone H2A/H2AX to regulate DNA repair<sup>63</sup>. Histones have been consistently detected in proteomic studies involving EVs<sup>64</sup>. Graham and colleagues demonstrated that EVs can transfer chromatin-like structures containing histone H2B<sup>65</sup>, which is associated with p53 function. The presence of histones and genomic DNA in EVs may result from micronuclei formation, a structure formed by cytoplasmic content surrounded by the nuclear envelope as a result of DNA damage during mitosis<sup>66</sup>. Although the precise role of histones in TNBC-derived EVs remains unclear, their presence in plasma may indicate that cancer cells are undergoing genomic instability, a hallmark of cancer<sup>67</sup>, or they could be transferred to recipient cells, where their function warrants further investigation.

Regardless of their mechanistic role, HISTH2A and HISTH2B emerged as strong TNBC diagnostic candidates, particularly HISTH2A, which was identified as exclusive to TNBC-derived EVs before surgery and significantly elevated compared to healthy conditions in our study. We demonstrated its overexpression in TNBC biopsies, distinguishing TNBC from benign lesions, Luminal, and HER2-amplified subtypes. Furthermore, we provide evidence of HISTH2A expression in TNBC cell lines, whereas hormone receptor-positive lines showed slight to no expression. Nevertheless, this requires further investigation as our cell line analysis was limited to only MDA-MB-231.

An intriguing finding is that immunological-related pathways were enriched following surgical intervention, similar to what was observed in healthy individuals, albeit through different proteins. This underscores the crucial role of immune cells in cancer progression and suggests a potential mechanism for immune evasion mediated by EVs. However, it is important to note that cancer surgery can trigger an inflammatory response, which has been associated with disease relapse<sup>68</sup>. Surgery procedures induce a wound response in the affected tissue, which leads to macrophage polarization<sup>69</sup>, platelet activation, and fibrin clot formation, all of which contribute to systemic inflammation<sup>68</sup>. Moreover, post-surgical inflammation can recruit and stimulate the proliferation of myeloid-derived suppressor cells (MDSCs) and regulatory T cells (Treg) populations, creating an immunosuppressive microenvironment<sup>68,70</sup>. Additionally, platelet activation can shield circulating tumor cells and promote metastasis<sup>71,72</sup>. In this context, our study provided information that combining surgery intervention with immunotherapy could be a promising therapeutic strategy. Furthermore, the unique or abundant proteins identified in our study post-surgery offer valuable insights for novel therapeutic applications targeting the immune modulation induced by surgery.

## Conclusion

Through proteomic analysis, we identified several exclusive or differentially expressed proteins in plasma-derived EVs that could serve as biomarkers for both benign and malignant conditions, with particular relevance to the TNBC subtype. Notably, immune system regulation emerged as a major process mediated by EVs, being enriched in healthy women and post-surgical intervention. This scenario provides new insights for immunotherapy as a combinatory strategy with cancer surgery. Additionally, HISTH2A was identified as a promising candidate for liquid biopsy in TNBC surveillance. However, the study faces limitations, including a restricted sample size and the focus on a limited number of centers, which may not fully represent the heterogeneity of the broader breast cancer population. Furthermore, the EVs analysis was conducted in a specific post-surgical context, potentially missing variations in the proteomic profile throughout different stages of treatment and disease progression. To overcome these limitations, future studies should include broader, multicentric sampling to validate the identified markers and assess population variability. Additionally, investigating the functional roles of the identified proteins, such as HISTH2A, is essential to better understand their clinical relevance and potential for disease monitoring. Lastly, further exploration of combining immunotherapy strategies with EVs analysis will be crucial in optimizing treatment protocols and improving patient outcomes in TNBC.

## Data availability

The data used to support the findings of this study are available from the corresponding author upon request.

Received: 18 September 2024; Accepted: 19 March 2025

Published online: 09 April 2025

## References

1. Sung, H. et al. Global cancer statistics 2020: GLOBOCAN estimates of incidence and mortality worldwide for 36 cancers in 185 countries. *CA Cancer J. Clin.* **71**, 209–249 (2021).
2. Goldhirsch, A. et al. Strategies for subtypes-dealing with the diversity of breast cancer: Highlights of the St. Gallen international expert consensus on the primary therapy of early breast cancer 2011. *Ann. Oncol.* **22**, 1736–1747 (2011).
3. Yin, L., Duan, J. J., Bian, X. W. & Yu, S. C. Triple-negative breast cancer molecular subtyping and treatment progress. *Breast Cancer Res.* **22**, 61 (2020).
4. Lacerda, J. Z. et al. Therapeutic potential of melatonin in the regulation of MiR-148a-3p and angiogenic factors in breast cancer. *Microna* **8**, 237–247 (2019).
5. Jardim-Perassi, B. V. et al. RNA-Seq transcriptome analysis shows anti-tumor actions of melatonin in a breast cancer xenograft model. *Sci. Rep.* **9**, 966 (2019).
6. de Godoy, B. L. V. et al. Synergistic actions of Alpelisib and melatonin in breast cancer cell lines with PIK3CA gene mutation. *Life Sci.* **324**, 121708 (2023).
7. Won, K. A. & Spruck, C. Trilateral breast cancer therapy: Current and future perspectives (Review). *Int. J. Oncol.* **57**, 1245–1261 (2020).
8. Tamarindo, G. H., Novais, A. A., Chuffa, L. G. A. & Zuccari, D. A. P. C. Metabolic alterations in canine mammary tumors. *Animal (Basel)* **13** 2757 (2023).
9. Kudelova, E. et al. Genetic heterogeneity, tumor microenvironment and immunotherapy in triple-negative breast cancer. *Int. J. Mol. Sci.* **23** 14937 (2022).
10. Sarhangi, N. et al. Breast cancer in the era of precision medicine. *Mol. Biol. Rep.* **49**, 10023–10037 (2022).
11. Mathai, R. A. et al. Potential utility of liquid biopsy as a diagnostic and prognostic tool for the assessment of solid tumors: Implications in the precision oncology. *J. Clin. Med.* **8** 373 (2019).
12. Colombo, J. et al. Liquid biopsy as a diagnostic and prognostic tool for women and female dogs with breast cancer. *Cancers (Basel)* **13** 5233 (2021).
13. Novais, A. A., Tamarindo, G. H., de Chuffa, L. G. & Zuccari, D. A. P. de C. Decoding hidden messengers: Proteomic profiling of exosomes in mammary cancer research. *Biomedicines* **11** 2839 (2023).
14. Bhatia, R., Chang, J., Munoz, J. L. & Walker, N. D. Forging new therapeutic targets: Efforts of tumor derived exosomes to prepare the pre-metastatic niche for cancer cell dissemination and dormancy. *Biomedicines* **11** 1614 (2023).
15. Graham, R. et al. Serum-derived extracellular vesicles from breast cancer patients contribute to differential regulation of T-cell-mediated immune-escape mechanisms in breast cancer subtypes. *Front. Immunol.* **14**, 1204224 (2023).

16. Wang, X. et al. Serum-derived extracellular vesicles facilitate Temozolomide resistance in glioblastoma through a HOTAIR-dependent mechanism. *Cell. Death Dis.* **13**, 344 (2022).
17. Xie, F. et al. Breast cancer cell-derived extracellular vesicles promote CD8+ T cell exhaustion via TGF- $\beta$  type II receptor signaling. *Nat. Commun.* **13**, 4461 (2022).
18. Brena, D., Huang, M. B. & Bond, V. Extracellular vesicle-mediated transport: Reprogramming a tumor microenvironment conducive with breast cancer progression and metastasis. *Transl Oncol.* **15**, 101286 (2022).
19. Dong, M., Liu, Q., Xu, Y. & Zhang, Q. Extracellular vesicles: The landscape in the progression, diagnosis, and treatment of triple-negative breast cancer. *Front. Cell. Dev. Biol.* **10**, 842898 (2022).
20. Lopatin, T. et al. Targeting IL-3Ra on tumor-derived endothelial cells blunts metastatic spread of triple-negative breast cancer via extracellular vesicle reprogramming. *Oncogenesis* **9**, 90 (2020).
21. Gelsomino, L. et al. Proteomic profiling of extracellular vesicles released by Leptin-Treated breast cancer cells: A potential role in cancer metabolism. *Int. J. Mol. Sci.* **23**, 12941 (2022).
22. Fong, M. Y. et al. Breast-cancer-secreted miR-122 reprograms glucose metabolism in premetastatic niche to promote metastasis. *Nat. Cell. Biol.* **17**, 183–194 (2015).
23. Novaïs, A. A. et al. Exploring canine mammary cancer through liquid biopsy: Proteomic profiling of small extracellular vesicles. *Cancers (Basel)* **16**, 2562 (2024).
24. Dorado, E. et al. Extracellular vesicles as a promising source of lipid biomarkers for breast cancer detection in blood plasma. *J. Extracell. Vesicles* **13**, e12419 (2024).
25. Lin, L. et al. Plasma-Derived extracellular vesicles circular RNAs serve as biomarkers for breast cancer diagnosis. *Front. Oncol.* **11**, 752651 (2021).
26. Chen, I. H. et al. Phosphoproteins in extracellular vesicles as candidate markers for breast cancer. *Proc. Natl. Acad. Sci. USA* **114**, 3175–3180 (2017).
27. da Silva, M. et al. Corpus luteum proximity alters molecular signature of the small extracellular vesicles and cumulus cells in the bovine ovarian follicle environment. *Mol. Cell. Endocrinol.* **592**, 112347 (2024).
28. Barcelos, S. M. et al. Extracellular vesicles derived from bovine adipose-derived mesenchymal stromal cells enhance in vitro embryo production from lesioned ovaries. *Cytotherapy* **26**, 1141–1151 (2024).
29. De Bem, T. H. C. et al. Biosensor capability of the endometrium is mediated in part, by altered MiRNA cargo from conceptus-derived extracellular vesicles. *FASEB J.* **38**, e23639 (2024).
30. da Silva Rosa, P. M. et al. Corpus luteum presence in the bovine ovary increase intrafollicular progesterone concentration: Consequences in follicular cells gene expression and follicular fluid small extracellular vesicles MiRNA contents. *J. Ovarian Res.* **17**, 65 (2024).
31. Cox, J. & Mann, M. MaxQuant enables high peptide identification rates, individualized p.p.b.-range mass accuracies and proteome-wide protein quantification. *Nat. Biotechnol.* **26**, 1367–1372 (2008).
32. Cox, J. et al. Andromeda: A peptide search engine integrated into the MaxQuant environment. *J. Proteome Res.* **10**, 1794–1805 (2011).
33. Tyanova, S., Cox, J. & Perseus A bioinformatics platform for integrative analysis of proteomics data in cancer research. *Methods Mol. Biol.* **1711**, 133–148 (2018).
34. Xia, J., Psychogios, N., Young, N. & Wishart, D. S. MetaboAnalyst: A web server for metabolomic data analysis and interpretation. *Nucleic Acids Res.* **37**, W652–W660 (2009).
35. Thomas, P. D. et al. Making genome-scale phylogenetics accessible to all. *Protein Sci.* **31**. PANTHER, 8–22 (2022).
36. Ashburner, M. et al. Gene ontology: Tool for the unification of biology. *Nat. Genet.* **25**, 25–29 (2000).
37. Gene Ontology Consortium. The gene ontology knowledgebase in 2023. *Genetics* **224**, iyad031 (2023).
38. Szklarczyk, D. et al. The STRING database in 2023: Protein-protein association networks and functional enrichment analyses for any sequenced genome of interest. *Nucleic Acids Res.* **51**, D638–D646 (2023).
39. Jensen, K., Krusenstjerna-Hafström, R., Lohse, J., Petersen, K. H. & Derand, H. A novel quantitative immunohistochemistry method for precise protein measurements directly in formalin-fixed, paraffin-embedded specimens: Analytical performance measuring HER2. *Mod. Pathol.* **30**, 180–193 (2017).
40. Varghese, F., Bukhari, A. B., Malhotra, R. & De, A. IHC profiler: An open source plugin for the quantitative evaluation and automated scoring of immunohistochemistry images of human tissue samples. *PLoS ONE* **9**, e96801 (2014).
41. Novaïs, A. A. et al. Small extracellular vesicles and survivin as diagnostic and prognostic marker for breast cancer: A pilot study. *Clin. Oncol. (Las Vegas)* **06**, 01–07 (2023).
42. Paepke, S., Metz, S., Brea Salvago, A. & Ohlinger, R. Benign breast tumours - Diagnosis and management. *Breast Care (Basel)* **13**, 403–412 (2018).
43. Román, M. et al. Long-Term risk of breast cancer after diagnosis of benign breast disease by screening mammography. *Int. J. Environ. Res. Public Health* **19**, 2625 (2022).
44. Wang, L. et al. BRAF V600E mutation in triple-negative breast cancer: A case report and literature review. *Oncol. Res. Treat.* **45**, 54–61 (2022).
45. Alhamdan, Y. R., Ayoub, N. M., Jaradat, S. K., Shatnawi, A. & Yaghan, R. J. BRAF expression and copy number alterations predict unfavorable tumor features and adverse outcomes in patients with breast cancer. *Int. J. Breast Cancer* **2024**, 6373900 (2024).
46. Bakker, N. A. M. et al. Triple-negative breast cancer modifies the systemic immune landscape and alters neutrophil functionality. *NPJ Breast Cancer* **11**, 5 (2025).
47. Taifour, T. et al. The tumor-derived cytokine Chi3l1 induces neutrophil extracellular traps that promote T cell exclusion in triple-negative breast cancer. *Immunity* **56**, 2755–2772e8 (2023).
48. Kim, I. S. et al. Immuno-subtyping of breast cancer reveals distinct myeloid cell profiles and immunotherapy resistance mechanisms. *Nat. Cell. Biol.* **21**, 1113–1126 (2019).
49. Meng, H. et al. ZG16 promotes T-cell mediated immunity through direct binding to PD-L1 in colon cancer. *Biomark. Res.* **10**, 47 (2022).
50. Meng, H., Ding, Y., Liu, E., Li, W. & Wang, L. ZG16 regulates PD-L1 expression and promotes local immunity in colon cancer. *Transl. Oncol.* **14**, 101003 (2021).
51. Wang, E., Qiang, X., Li, J., Zhu, S. & Wang, P. The in vitro immune-modulating properties of a sweat gland-derived antimicrobial peptide dermcidin. *Shock* **45**, 28–32 (2016).
52. Brauer, H. A. et al. Dermcidin expression is associated with disease progression and survival among breast cancer patients. *Breast Cancer Res. Treat.* **144**, 299–306 (2014).
53. Bancovik, J. et al. Dermcidin exerts its oncogenic effects in breast cancer via modulation of ERBB signaling. *BMC Cancer* **15**, 70 (2015).
54. Lane, D. M., Boatman, K. K. & McConathy, W. J. Serum lipids and apolipoproteins in women with breast masses. *Breast Cancer Res. Treat.* **34**, 161–169 (1995).
55. Mosapour, A., Tehrani, K., Atri, M. & F. S. & Expression level of VLDL receptor and VLDL-c levels in the malignant and benign breast tumors: The correlation with miRNA-4465 and miRNA-1297. *Mol. Cell. Probes* **53**, 101624 (2020).
56. Maran, L., Hamid, A. & Hamid, S. B. S. Lipoproteins as markers for monitoring cancer progression. *J. Lipids* **2021** 8180424 (2021).
57. Tamarindo, G. H. et al. The polyunsaturated fatty acid docosahexaenoic affects mitochondrial function in prostate cancer cells. *Cancer Metab.* **12**, 24 (2024).

58. Tamarindo, G. H., Gobbo, M. G., Taboga, S. R., Almeida, E. A. & Góes, R. M. Melatonin ameliorates degenerative alterations caused by age in the rat prostate and mitigates high-fat diet damages. *Cell. Biol. Int.* **45**, 92–106 (2021).
59. Wang, G. et al. Lung cancer scRNA-seq and lipidomics reveal aberrant lipid metabolism for early-stage diagnosis. *Sci. Transl Med.* **14**, eabk2756 (2022).
60. Kouba, S. et al. Lipid metabolism and calcium signaling in epithelial ovarian cancer. *Cell. Calcium.* **81**, 38–50 (2019).
61. Zippinotti, D. et al. The impact of lipid metabolism on breast cancer: A review about its role in tumorigenesis and immune escape. *Cell. Commun. Signal.* **21**, 161 (2023).
62. Klinge, C. M. Estrogen receptor interaction with Estrogen response elements. *Nucleic Acids Res.* **29**, 2905–2919 (2001).
63. Lee, S. O. et al. UBA80 and UBA52 fine-tune RNF168-dependent histone ubiquitination and DNA repair. *J. Biol. Chem.* **299**, 105043 (2023).
64. Ortiz, A. Not all extracellular vesicles were created equal: Clinical implications. *Ann. Transl. Med.* **5**, 111 (2017).
65. Ghanam, J. et al. Extracellular vesicles transfer chromatin-like structures that induce non-mutational dysfunction of p53 in bone marrow stem cells. *Cell. Discov.* **9**, 12 (2023).
66. Yokoi, A. et al. Mechanisms of nuclear content loading to exosomes. *Sci. Adv.* **5**, eaax8849 (2019).
67. Fenech, M. Cytokinesis-block micronucleus cytome assay. *Nat. Protoc.* **2**, 1084–1104 (2007).
68. Cheng, X., Zhang, H., Hamad, A., Huang, H. & Tsung, A. Surgery-mediated tumor-promoting effects on the immune microenvironment. *Semin. Cancer Biol.* **86**, 408–419 (2022).
69. Tham, M. et al. Macrophage depletion reduces postsurgical tumor recurrence and metastatic growth in a spontaneous murine model of melanoma. *Oncotarget* **6**, 22857–22868 (2015).
70. Sun, Z., Du, C., Xu, P. & Miao, C. Surgical trauma-induced CCL18 promotes recruitment of regulatory T cells and colon cancer progression. *J. Cell. Physiol.* **234**, 4608–4616 (2019).
71. Anvari, S., Osei, E. & Maftoon, N. Interactions of platelets with circulating tumor cells contribute to cancer metastasis. *Sci. Rep.* **11**, 15477 (2021).
72. Zhou, L. et al. The critical role of platelet in cancer progression and metastasis. *Eur. J. Med. Res.* **28**, 385 (2023).

## Acknowledgements

The authors thank to Dr. Thais Cataldi Regiani and Dr. Carlos Alberto Labate from the Max Feffer Genetics of Plants Laboratory (Escola Superior de Agricultura Luiz de Queiroz, University of São Paulo, Piracicaba, São Paulo, Brazil) staff for their expertise and assistance in processing and collecting proteomics data; Dr. Jucimara Colombo and to the hospital staff for sample collection for this research.

## Author contributions

G.H.T., A.A.N. and D.A.P.C.Z. contributed to the conception and design of the work. G.H.T., A.A.N., B.M.F., D.L.A., A.A., C.A.S., N.A.B.Jr, J.C.S. and F.F.S. contributed to material preparation, data collection and analysis. The first draft of the manuscript was written by G.H.T. with contributions of A.A.N, L.G.A.C. and D.A.P.C. All authors approved the final manuscript.

## Funding

This research was supported by São Paulo Research Foundation (FAPESP), Grant number 2021/12970-8 awarded to D.A.P.C.

## Declarations

### Competing interests

The authors declare no competing interests.

### Informed consent

Informed consent was obtained from all participants and/or their legal guardians.

### Additional information

**Supplementary Information** The online version contains supplementary material available at <https://doi.org/10.1038/s41598-025-95232-2>.

**Correspondence** and requests for materials should be addressed to D.A.P.C.Z.

**Reprints and permissions information** is available at [www.nature.com/reprints](http://www.nature.com/reprints).

**Publisher's note** Springer Nature remains neutral with regard to jurisdictional claims in published maps and institutional affiliations.

**Open Access** This article is licensed under a Creative Commons Attribution-NonCommercial-NoDerivatives 4.0 International License, which permits any non-commercial use, sharing, distribution and reproduction in any medium or format, as long as you give appropriate credit to the original author(s) and the source, provide a link to the Creative Commons licence, and indicate if you modified the licensed material. You do not have permission under this licence to share adapted material derived from this article or parts of it. The images or other third party material in this article are included in the article's Creative Commons licence, unless indicated otherwise in a credit line to the material. If material is not included in the article's Creative Commons licence and your intended use is not permitted by statutory regulation or exceeds the permitted use, you will need to obtain permission directly from the copyright holder. To view a copy of this licence, visit <http://creativecommons.org/licenses/by-nc-nd/4.0/>.

© The Author(s) 2025